Geology of the Derain quadrangle (H10), Mercury

Christopher C Malliband, David A Rothery, Matthew R Balme, Susan J Conway, David L Pegg, Jack Wright

Taylor & Francis
Taylor & Francis Group

Journal of Maps

ISSN: (Print) (Online) Journal homepage: https://www.tandfonline.com/loi/tjom20

Geology of the Derain quadrangle (H10), Mercury

Christopher C. Malliband, David A. Rothery, Matthew R. Balme, Susan J. Conway, David L. Pegg & Jack Wright

To cite this article: Christopher C. Malliband, David A. Rothery, Matthew R. Balme, Susan J. Conway, David L. Pegg & Jack Wright (2022): Geology of the Derain quadrangle (H10), Mercury, Journal of Maps, DOI: 10.1080/17445647.2022.2112774

To link to this article: https://doi.org/10.1080/17445647.2022.2112774

JOURNAL OF MAPS
https://doi.org/10.1080/17445647.2022.2112774

Geology of the Derain quadrangle (H10), Mercury

Christopher C. Malliband[a], David A. Rothery [a], Matthew R. Balme [a], Susan J. Conway [b], David L. Pegg[a] and Jack Wright [a,c]

[a]Department of Physical Sciences, The Open University, Walton Hall, Milton Keynes, UK; [b]CNRS, UMR 6112 Laboratoire de Planétologie et Géodynamique, Université de Nantes, Nantes, France; [c]European Space Agency / ESAC, Madrid, Spain

ABSTRACT

We present the results of geological mapping of Mercury's Derain (H10) quadrangle (0°-72°E and 22.5°N-22.5°S) using data from the MESSENGER spacecraft. The map is presented on a scale of 1:3,000,000, for which linework was drawn at 1:300,000. We distinguish three major morphological plains units: Smooth, Intermediate, and Intercrater Plains. We produced two versions of the map, with craters classified according to a 3- and 5-class degradation system. This allows compatibility with other MESSENGER-era maps and Mariner 10-era maps. This map will help provide science context for the ESA-JAXA BepiColombo mission to Mercury.

ARTICLE HISTORY
Received 24 March 2022
Revised 4 August 2022
Accepted 8 August 2022

KEYWORDS
Mercury; planetary geology; Derain; impact processes; planetary resurfacing

1. Introduction

Mercury has been studied by three spacecraft, Mariner 10 (flybys 1974–1975), MESSENGER (MErcury, Surface, Space ENvironment, GEochemistry, and Ranging; flybys 2008–2009, in orbit 2011–2015) and BepiColombo (first flyby October 2021, orbit insertion due December 2025). For mapping purposes, Mercury is divided into 15 quadrangles of similar size. Due to orbital and illumination constraints, Mariner 10 imaged only approximately 50% of Mercury's surface. This allowed geological maps to be made at 1:5 million scale of the complete H03, H06, H07, H11 and H12 quadrangles, with partial coverage of the H01, H02, H08, and H15 quadrangles.

MESSENGER obtained global image coverage, allowing complete mapping of all quadrangles. A 1:15 million scale global geological map has been produced by members of the MESSENGER team (Kinczyk et al., 2018; Prockter et al., 2016), but the quality of MESSENGER image data is sufficient for larger scale (1:3M) maps to be produced covering the entire globe. Hitherto, post-MESSENGER geological maps of the H02 (Galluzzi et al., 2016), H03 (Guzzetta et al., 2017), H04 (Mancinelli et al., 2016), H05 (Wright et al., 2019) H06 (Giacomini et al., 2022) and H14 (Pegg et al., 2021) quadrangles have been published. We use the term geological map to be consistent with descriptions of those previous maps, although all are strictly morphostratigraphic maps as mapping is based principally on geomorphology. Here, we describe our geological map of the H10 (Derain) quadrangle.

2. Data

2.1. Basemaps

We used a variety of basemaps (Figure 1), produced the MESSENGER team, using the MDIS (Mercury Dual Imaging System) narrow- and wide-angle cameras (NAC/WAC) (Hawkins et al., 2007). Most were released in an equirectangular projection having been placed on the 2015 Mercury datum with a planetocentric radius of 2,439,400 m, controlled and projected onto the global digital elevation model (DEM).

2.1.1. BDR (Basemap reduced data record) 166 mpp mosaic basemap

The primary mosaic for mapping was the BDR monochrome basemap with an average resolution of 166 mpp (metres per pixel) (Figure 1(A)). This is the highest resolution and most recent mosaic, composed of images from the NAC and WAC with predominantly moderate incidence angle close to 74°. This allows good visibility of features with topographic relief, and was the primary dataset used in the production of the map.

2.1.2. BDR 250 mpp mosaic basemap

The 250 mpp mosaic is the predecessor moderate incidence angle mosaic to the BDR 166 mpp mosaic and was produced earlier in the MESSENGER mission. It has a lower spatial resolution than the 166 mpp BDR basemap but can occasionally be more coherent, with fewer joins, misregistration and changes in viewing geometry, over small areas. As it was produced earlier in the

CONTACT David A. Rothery david.rothery@open.ac.uk Department of Physical Sciences, The Open University, Walton Hall, Milton Keynes, MK6 4AJ, UK

Supplemental map for this article can be accessed at https://doi.org/10.1080/17445647.2022.2112774.

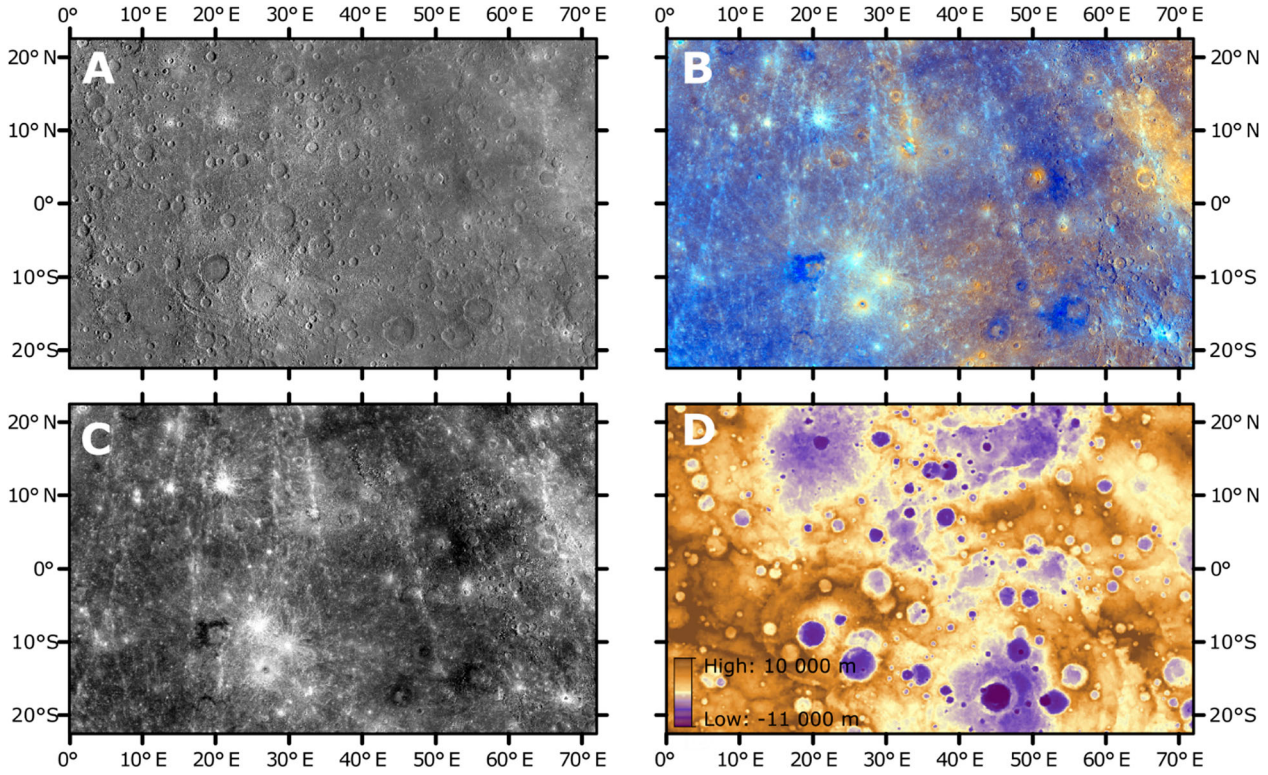

Figure 1. Principal basemaps used in the preparation of the geological map of the Derain Quadrangle. (A) BDR 166 mpp average basemap. (B) The enhanced colour basemap (Denevi et al., 2018). (C) Low incidence angle basemap. D: USGS global DEM from stereo imagery (Becker et al., 2016).

MESSENGER mission, it is projected using the 2010 datum with a radius of 2,440,000 m. This was not topographically controlled and instead projected onto a simple sphere, so we manually referenced any linework mapped using this mosaic onto the 2015 datum.

2.1.3. Low incidence angle 166 mpp mosaic

The low incidence angle basemap is a mosaicked data set composed of low incidence angle (i.e. small angle between the sun and surface normal) images (Figure 1(C)). Low incidence angle imagery accentuates albedo differences and minimizes obscuration by shadows, but surface relief and texture are difficult to see.

2.1.4. High incidence angle (east- and west-facing) 166 mpp mosaics

These high incidence angle mosaics comprise images with an incidence angle of close to 78°, with consistent illumination from east or west. These basemaps were useful for revealing detail within areas shadowed on the BDR mosaic.

2.1.5. Enhanced colour 665 mpp mosaic

'Enhanced color' is a standard MESSENGER product that accentuates subtle colour differences (Figure 1(B)). It was created using MDIS-WAC images in the 430, 750, 1000 nm bands. Principal component analysis was completed in this spectral space by the MESSENGER team. The second principal component is placed in the red, the first principal component in the green, and the ratio of 430/1000 nm bands in the blue channel, respectively (Denevi et al., 2009; Denevi et al., 2018).

Enhanced colour helps provide spectral context for morphological observations and can sometimes be used to distinguish plains types (Denevi et al., 2013; Whitten et al., 2014). It is invaluable for mapping spectrally distinct surficial features such as faculae, most of which are probably explosive volcanic deposits (Prockter et al., 2010), and fields of hollows (Blewett et al., 2011).

2.1.6. 665 mpp stereo digital elevation model

The only topographic product that covers the whole of the Derain quadrangle is the global stereo-derived ~665 mpp DEM (Becker et al., 2016) (Figure 1(D)). MDIS had no inbuilt stereoscopic capability, so the DEM was created using unsupervised computer selection of image pairs acquired under different lighting conditions. The DEM was then verified using elevation data from the Mercury Laser Altimeter on MESSENGER (Becker et al., 2016). In our mapping, we used the DEM mainly to help map lobate scarps and characterise the intercrater plains unit (Section 4.4.1).

3. Methods

3.1. Projection

We used a Mercator projection, as is conventional for mapping equatorial regions of planetary bodies, and used the USGS 2015 datum.

3.2. Map standards

We drew the map to be consistent with previous MESSENGER-era Mercury maps (Galluzzi et al., 2016; Giacomini et al., 2022; Guzzetta et al., 2017; Mancinelli et al., 2016; Pegg et al., 2021; Wright et al., 2019), and PlanMap standards (van der Bogert et al., 2020), which are based on those of the USGS (Tanaka et al., 2011).

3.2.1. Map scale

We prepared the map for publication at 1:3 million scale and, for reasons elaborated by Wright et al. (2019), drew linework at a scale of 1:400,000. For consistency, we drew linework primarily using vertex streaming with 500 m spacing.

3.2.2. Reconciliation with adjacent maps

We extended our mapping 5° beyond the quadrangle to assist the eventual creation of a global Mercury geological map and reconciled our linework with adjacent quadrangles H05 and H14.

3.3. Crater classification

Following the approach of previous maps, such as Galluzzi et al. (2016), we mapped all craters exceeding 5 km in diameter, and classified the degradation state and mapped the ejecta for craters with a diameter greater than 20 km.

Mariner 10 maps (De Hon et al., 1981; Grolier & Boyce, 1984; Guest & Greeley, 1983; King & Scott, 1990; Schaber & McCauley, 1980; Trask & Dzurisin, 1984; Trask & Guest, 1975) divided craters into five degradation states, loosely following the divisions on the Moon. The least degraded class in the system is c_5, and the most degraded c_1 (Figure 2). This system was revisited and a full classification schema was produced in the MESSENGER era (Kinczyk et al., 2020).

Previous mappers have found that when using the 5-class degradation states, there are occasional local contradictions between relative ages as implied by degradation state and superposition relationships (Galluzzi et al., 2016). They eliminate most of these by resorting to a simpler 3-class system, C_3-C_1 (Figure 3), which also improves reproducibility for integration between maps.

In common with Wright et al. (2019) and Pegg et al. (2021), we produced alternate versions of our map, using the 5- and 3-class systems (distinguished by the use of uppercase C for the 3-class system, and lowercase c for the 5-class system). This allows integration with other recent 3-class maps, and comparison with the global geological and Mariner 10 maps.

4. Description of map elements

4.1. Contacts

We classified contacts between (or, rarely, within) units into three types, based on the clarity of the contact. We mapped contacts as 'certain' where the position of a geological contact can be defined as within 500 m. 'Approximate' contacts were mapped where a contact can be seen to exist, but its exact location cannot be determined to within 500 m. We use a 'gradational' contact symbol sparingly where its location is particularly ill-defined, or its existence in doubt; in H10 this applies only to some boundaries of the Intermediate Plains unit (see below). Where the boundary between units is defined by a tectonic feature, such as a lobate scarp, the boundary is marked with the tectonic feature's ornamentation and can be considered a certain contact.

4.2. Crater rims

We mapped the rims of all craters with diameter >5 km, and distinguished the rims of those with diameter >20 km by use of a double hatchured ornamentation. Rather than mapping craters belonging to clear and obvious secondary fields or chains individually, we grouped them as secondary chains or fields to avoid cluttering the map and to show the geological relationships better. Rims of flooded or subdued craters, where the outline of a crater can be seen without any discernible ejecta or interior unit, are symbolized separately.

4.3. Tectonic features

The most common type of tectonic feature mapped is lobate scarps, which we show as thrusts based on their asymmetry. The ornamentation points in the direction of fault dip. We classified these as either certain or probable, depending on confidence of identification.

The other type of tectonic feature mapped is wrinkle ridges, which are more subtle ridges, also thought to be related to underlying faults. We distinguished two types: linear and rings, following Wright et al. (2019). Unlike other mapped quadrangles, H10 has no grabens long enough to be seen at the publication scale, and so these are absent from the map.

4.4. Mapped units

4.4.1. Intercrater plains (icp)

Intercrater Plains are the most extensive plains unit on Mercury (Whitten et al., 2014). They are heavily cratered, and although they can be crater-saturated, most examples are not. Crater morphologies show the full range of sizes and degradation state.

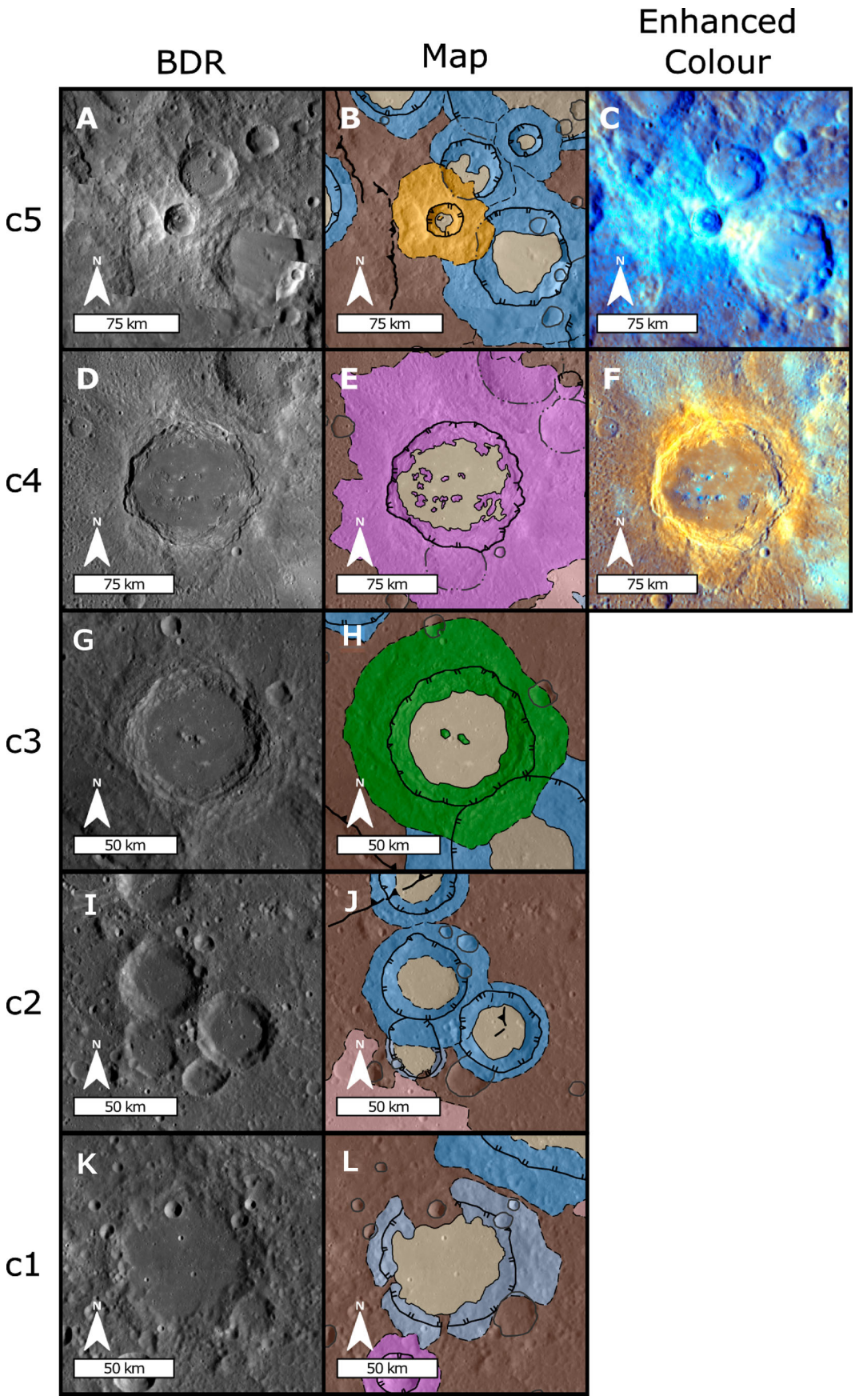

Figure 2. Examples of the 5-class crater degradation states. A, D, G, I and K show the craters in the BDR basemap. B, E, H, J and L show them as mapped. C and F show c5 and c4 craters in enhanced colour, because the presence or absence of albedo rays is the key distinguisher between these crater classes. Albedo features are not used to distinguish between any other crater classes.

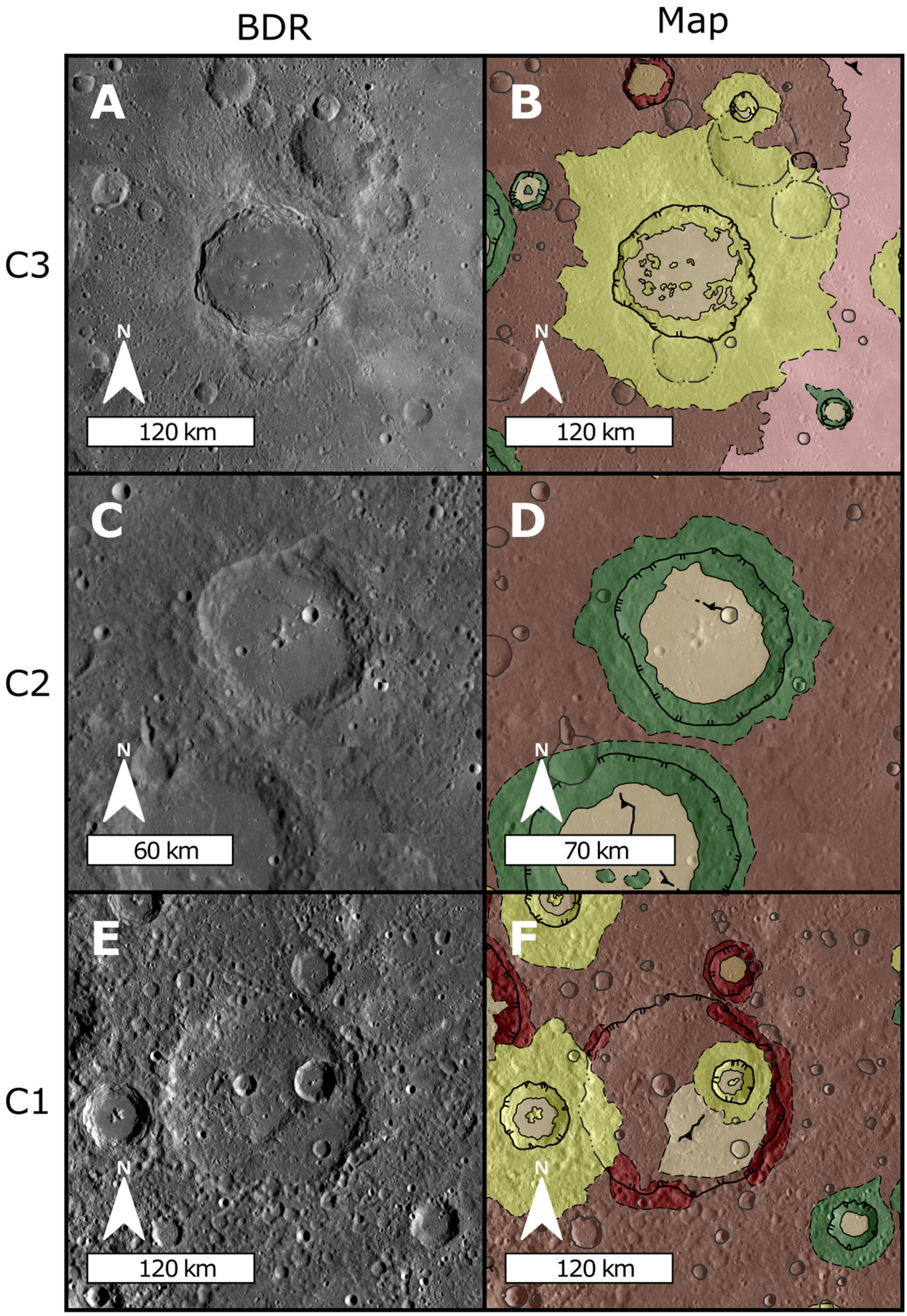

Figure 3. Examples of the three-class crater degradation states. A, C and E show the exemplar craters in the BDR basemap. B, D and F show the craters as mapped. The map colours follow the three crater class map sheet.

Topography on 50 km wavelengths is generally flat or gently rolling. Tectonism is expressed by lobate scarps, with no wrinkle ridges discernible. In enhanced colour, Intercrater Plains can be either red or blue, and they usually have relatively low reflectance. An example area is shown in Figure 4.

Intercrater Plains are generally interpreted to be heavily reworked volcanic plains. They may have originally looked much like smooth plains (Whitten et al., 2014) but have been heavily modified by cratering since emplacement. Intercrater Plains will therefore include a significant amount of reworked impact ejecta alongside the original volcanic material.

4.4.2. Intermediate plains (imp)

This is a plains unit geomorphically intermediate in texture and km-scale roughness between Smooth Plains and Intercrater Plains. We mapped Intermediate Plains where the majority of craters are subdued or mantled. Interiors of such craters may contain very small (<500 km^2) smooth patches, which, to avoid unnecessary complexity, we did not distinguish from the surrounding Intermediate Plains. The gradational boundaries of Intermediate Plains with other plains units sometimes make precise contacts difficult to locate.

The majority of intermediate plains have a mantled appearance and may represent thin or partial cover of an older (icp) surface by smooth material. The area of intermediate plains north-east of Apārangi Planitia lacks small smooth patches and may instead represent a unit whose age is intermediate between those of the nearby smooth and intercrater plains. An example of this type is shown in Figure 5.

While the intermediate plains have been questioned as being part of the global stratigraphy (Whitten et al., 2014), there is significant variation in plains units across the Derain quadrangle. Therefore we feel it useful to include this morphologically intermediate unit to best reflect the observable geomorphology within the quadrangle. It is likely that some examples of intermediate plains in H10 are a temporally intermediate unit (e.g. Giacomini et al., 2022), whereas others are a younger plains unit that is too thin to have fully obscured an underlying heavily cratered unit (e.g. Wright et al., 2019).

4.4.3. Smooth plains (sp)

Smooth Plains are characterised by a paucity of superimposed impact craters and a smooth texture. Those craters that do superpose smooth plains typically have well-developed ejecta blankets and appear morphologically fresh. Large expanses of sp such as Apārangi Planitia generally have sharp boundaries with intercrater plains, which they can be seen to overlie. Smaller areas can instead have gradational boundaries. Some smooth plains are differentiated in the enhanced colour mosaic by a red colour, most clearly in the case of Apārangi Planitia. Within the area of Smooth Plains south of Calypso Rupes, we identified patches of contrasting texture possibly relating to different episodes of lava flooding, which we distinguished by conventional contact symbology. Detail of Smooth Plains in Apārangi Planitia is shown in Figure 6.

Smooth Plains are likely the most recent large-scale effusive volcanic plains units (i.e. lava) on Mercury. Small smooth patches near large fresh craters most likely represent impact melt, and it is possible that some isolated patches of Smooth Plains may also be related to impact processes.

4.4.4. Crater materials

Crater materials units encompass a crater's continuous ejecta, terracing, and peak elements. In older degraded craters, continuous ejecta cannot be easily distinguished, and instead, the raised rim of the crater is mapped.

4.4.4.1. Heavily degraded craters: C_1 – three class, c_1 and c_2 – five class. These are the most degraded crater material mapped, and lack continuous ejecta deposits. The crater rim is usually heavily modified and may be discontinuous. Crater floors are often extensively modified. Peak elements are no longer identifiable. In the five-class system, c2 craters still retain identifiable crater walls, whereas c1 crater materials are scarcely discernible from background plains (Figure 2).

4.4.4.2. Degraded craters: C_2 – three class, c_3 – five class. These are craters in an intermediate degradation state, indicating a younger age than the preceding class. Crater rims are always continuous. Typically craters retain some areas of continuous ejecta, but this lacks a radial texture. Slumped internal terracing is common. Where craters are large enough, peak elements are still present but are typically slumped or otherwise degraded.

4.4.4.3. Fresh craters: C_3 – three class, c_4 and c_5 – five class. These are least degraded, and youngest, classes. They have clearly defined terracing, continuous ejecta with radial texture, and larger craters may be sources of chains of secondary impacts. Rims are sharp, and the crater floor is usually pristine. In the five-class system c_4 craters do not have rays but c_5 craters retain them.

4.4.5. Crater floor material

4.4.5.1. Smooth crater floor material (cfs). This is smooth material resembling smooth plains confined to crater floors. In fresh craters, this is generally interpreted as representing ponding of impact melt (Daniels, 2018; Wright et al., 2019). In older craters, this may be later volcanic plains.

4.4.5.2. Hummocky crater floor material (cfh). This is rough textured, often rolling material confined to

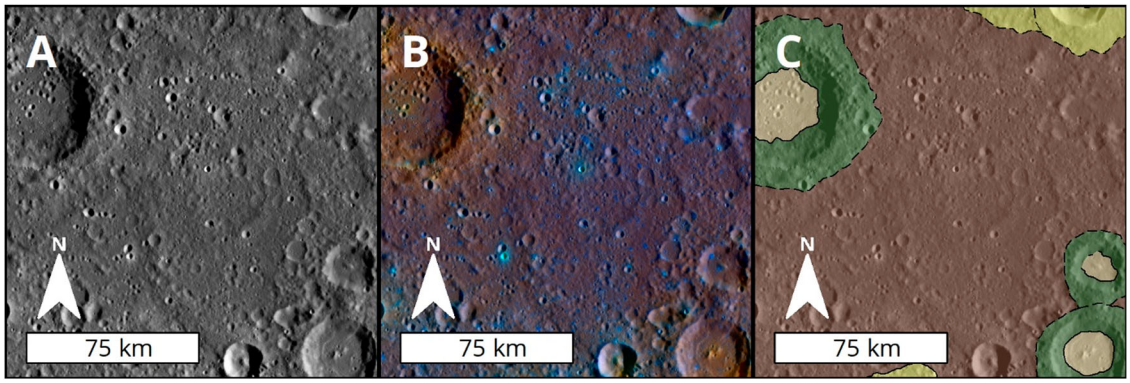

Figure 4. Area of intercrater plains at 40°E, 9°S. (A) BDR basemap mosaic, (B) Enhanced colour, (C) As mapped on the three crater class map sheet. The unit is heavily cratered, with many large and small craters showing various states of degradation.

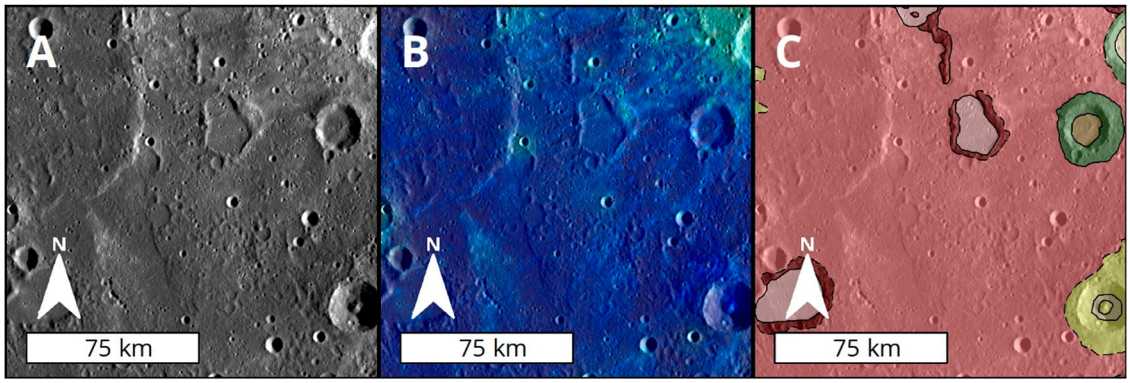

Figure 5. Area of intermediate plains at 19°E, 9°N shown in (A) BDR basemap mosaic; (B) enhanced colour; (C) as mapped on the three crater class map sheet. This area shows gentle rolling terrain with clearly subdued craters (C1 degradation), small lobate scarps and textural variation.

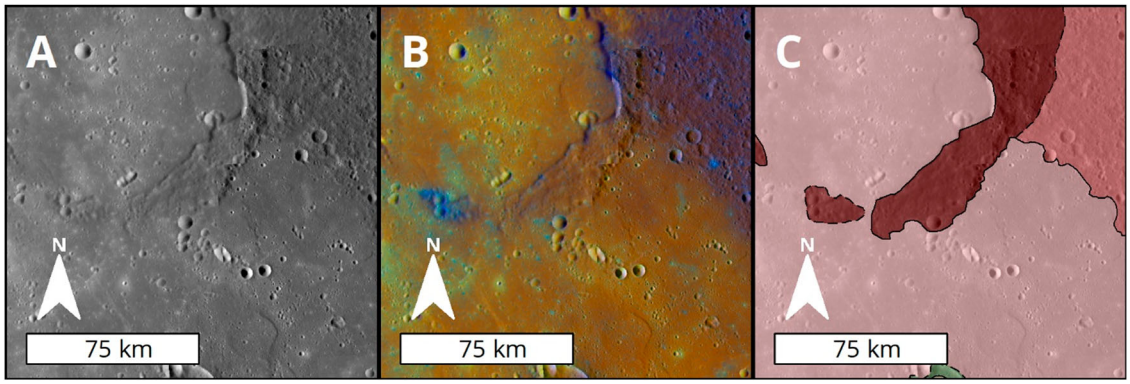

Figure 6. Area of smooth plains at 65°E, 14°N. The smooth plains are embaying a C1 crater. (A) BDR basemap mosaic. (B) Enhanced colour basemap mosaic, this area has the archetypal high reflectance red colour. (C) As mapped on the three crater class map sheet.

crater floors. It could represent degraded smooth floor material (Galluzzi et al., 2016) in more degraded craters, or collapsed debris, or crater floor that has not been covered by ponded impact melt.

4.5. Superficial units

We mapped superficial units, distinguished by textures or features that overprint the main geomorphological units. These include two classes of landforms associated with Mercury's volatile history: hollows, small, flat-floored, rimless depressions that are high albedo blue in enhanced colour imagery, and faculae, high albedo red albedo features in enhanced colour. Most faculae are thought to be explosive volcanic deposits, and these contain irregularly shaped pits, whose edges we mapped, thought to be volcanic vents. For consistency with previously

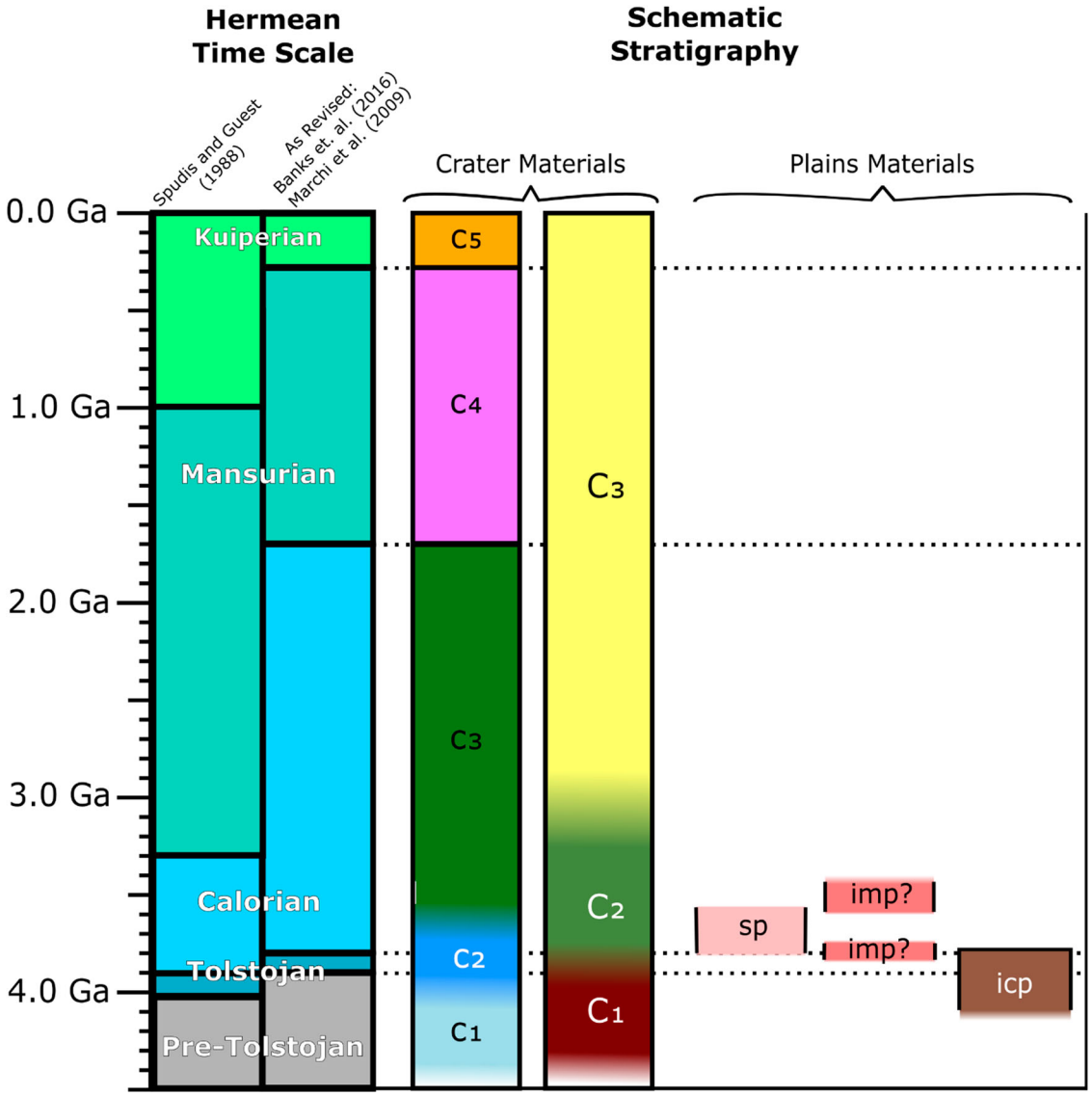

Figure 7. Schematic stratigraphy of the H-10 quadrangle. Smooth Plains – sp, Intermediate Plains – imp, Intercrater Plains – icp. As crater degradation is not always linear on Mercury age estimates are given for the main population of these craters. Alternative time periods from Spudis and Guest (1988) and following the revisions of Banks et al. (2017) using the crater production of Marchi et al. (2009), with midpoints used where ranges are given.

published maps, we included faculae with unusual morphology known as 'pitted ground' (Thomas et al., 2014), which occur in the Derain basin, within the same unit.

We also mapped secondary crater chains and bright crater rays as surficial units.

5. Correlation of units

We have constructed schematic stratigraphies for each version of the map, as shown in Figure 7. For dating of crater materials, we used accepted age estimates for the three-class system and for c_1-c_3 in the five-class system (e.g. Galluzzi et al., 2016; Wright et al., 2019). For c_4 and c_5 craters, we used ages derived from global population crater counts of such craters (Banks et al., 2017; Ernst et al., 2017). Emplacement age estimates for Smooth Plains were obtained from Byrne et al. (2016), and for the Intercrater Plains from Marchi et al. (2013). Ages tally with plains ages in Giacomini et al. (2022), except that we agree with Wright et al. (2019) in recognising that some Intermediate Plains could be younger than most Smooth Plains.

6. Summary

We present a geological map constructed using MESSENGER data covering the H10 quadrangle of Mercury, consistent with other published MESSENGER era maps. We mapped crater degradation with both currently used schemes. We mapped Intermediate Plains units, in common with previously published quadrangle maps, but in contrast to the current global map. This unit may be difficult to map consistently on a global scale, but it is necessary to best represent the plains units apparent at the quadrangle level. This

mapping will be useful in providing science context and targets for the ESA-JAXA BepiColombo orbital campaign at Mercury.

Software

We retrieved all datasets from NASA's Planetary Data System (https://pds-imaging.jpl.nasa.gov/portal/) and processed them to GIS-ready format through USGS ISIS3 software. We completed mapping using ESRI ArcGIS 10.5 and ArcPro software.

Acknowledgements

CCM and DLP acknowledge studentships from the Science and Technology Research Council, and funding from the Open University Space Strategic Research Area. CCM, DAR, MRB, DLP, and JW acknowledge the European Union's Horizon 2020 research and innovation programme under grant agreement No 776276 'Planmap'. SJC thanks the French Space Agency CNES for supporting her BepiColombo related work. All the authors thank Heike Apps, Valentina Galluzzi and Ivan Lopez for their insightful reviews of the text and map.

Disclosure statement

No potential conflict of interest was reported by the author(s).

Funding

This work was supported by European Commission [grant number 776276]; Science and Technology Facilities Council; Centre National d'Études Spatiales.

Data availability statement

Digital copies of the shape files and basemaps can be found here: https://zenodo.org/record/6957815#.Yupt5RzMLcs (3 crater classes); and https://zenodo.org/record/6957498#.YupmhBzMLcs (5 crater classes).

ORCID

David A. Rothery http://orcid.org/0000-0002-9077-3167
Matthew R. Balme http://orcid.org/0000-0001-5871-7475
Susan J. Conway http://orcid.org/0000-0002-0577-2312
Jack Wright http://orcid.org/0000-0003-0481-0863

References

Banks, M. E., Xiao, Z., Braden, S. E., Barlow, N. G., Chapman, C. R., Fassett, C. I., & Marchi, S. S. (2017). Revised constraints on absolute age limits for Mercury's Kuiperian and Mansurian stratigraphic systems. *Journal of Geophysical Research: Planets*, *122*(5), 1010–1020. https://doi.org/10.1002/2016JE005254

Becker, K. J., Robinson, M. S., Becker, T. L., Weller, L. A., Edmundson, K. L., Neumann, G. A., Perry, M. E., & Solomon, S. C. (2016). First global digital elevation model of mercury. In *47th lunar and planetary science conference* (p. 2959). Abstract No. 1903.

Blewett, D. T., Chabot, N. L., Denevi, B. W., Ernst, C. M., Head, J. W., Izenberg, N. R., Murchie, S. L., Solomon, S. C., Nittler, L. R., McCoy, T. J., Xiao, Z., Baker, D. M. H., Fassett, C. I., Braden, S. E., Oberst, J., Scholten, F., Preusker, F., & Hurwitz, D. M. (2011). Hollows on mercury: MESSENGER evidence for geologically recent volatile-related activity. *Science*, *333*(6051), 1856–1859. https://doi.org/10.1126/science.1211681

Byrne, P. K., Ostrach, L. R., Fassett, C. I., Chapman, C. R., Denevi, B. W., Evans, A. J., Klimczak, C., Banks, M. E., Head, J. W., & Solomon, S. C. (2016). Widespread effusive volcanism on mercury likely ended by about 3.5 Ga. *Geophysical Research Letters*, *43*(14), 7408–7416. https://doi.org/10.1002/2016GL069412

Daniels, J. W. (2018). *Impact melt emplacement on Mercury*. Western Libraries Electronic Thesis and Dissertation Repository. No. 5657.

De Hon, R. A., Scott, D. H., & Underwood, J. R. Jr. (1981). Geologic Map of the Kuiper (H-6) Quadrangle of Mercury. United States Geological Survey, Geologic Investigations Series, Map I-1233.

Denevi, B. W., Chabot, N. L., Murchie, S. L., Becker, K. J., Blewett, D. T., Domingue, D. L., Ernst, C. M., Hash, C. D., Hawkins, S. E., Keller, M. R., & Laslo, N. R. (2018). Calibration, projection, and final image products of MESSENGER's mercury dual imaging system. *Space Science Reviews*, *214*(1), 1–52. https://doi.org/10.1007/s11214-017-0440-y

Denevi, B. W., Ernst, C. M., Meyer, H. M., Robinson, M. S., Murchie, S. L., Whitten, J. L., Head, J. W., Watters, T. R., Solomon, S. C., Ostrach, L. R., Chapman, C. R., Byrne, P. K., Klimczak, C., & Peplowski, P. N. (2013). The distribution and origin of smooth plains on mercury. *Journal of Geophysical Research: Planets*, *118*(5), 891–907. https://doi.org/10.1002/jgre.20075

Denevi, B. W., Robinson, M. S., Solomon, S. C., Murchie, S. L., Blewett, D. T., Domingue, D. L., McCoy, T. J., Ernst, C. M., Head, J. W., Watters, T. R., & Chabot, N. L. (2009). The evolution of mercury's crust: A global perspective from MESSENGER. *Science*, *324*(5927), 613–618. https://doi.org/10.1126/science.1172226

Ernst, C. M., Denevi, B. W., & Ostrach, L. R. (2017). Updated absolute age estimates for the Tolstoj and caloris Basins, Mercury. In *48th lunar and planetary science conference* (p. 2934). Abstract No. 1964.

Galluzzi, V., Guzzetta, L., Ferranti, L., Di Achille, G., Rothery, D. A., & Palumbo, P. (2016). Geology of the Victoria quadrangle (H02), Mercury. *Journal of Maps*, *12*(sup1), 227–238. https://doi.org/10.1080/17445647.2016.1193777

Giacomini, L., Galluzzi, V., Massironi, M., Ferranti, L., & Palumbo, P. (2022). Geology of the Kuiper quadrangle (H06), Mercury. *Journal of Maps*. Advance online publication. https://doi.org/10.1080/17445647.2022.2035268

Grolier, M. J., & Boyce, J. M. (1984). Geologic map of the Borealis region (H-1) of Mercury. USGS Miscellaneous investigations series Map I–1660 21.

Guest, J. E., & Greeley, R. (1983). Geologic map of the Shakespeare (H-3) quadrangle of Mercury. USGS Miscellaneous Investigations Series, Map I-1408.

Guzzetta, L., Galluzzi, V., Ferranti, L., & Palumbo, P. (2017). Geology of the Shakespeare quadrangle (H03), Mercury. *Journal of Maps*, *13*(2), 227–238. https://doi.org/10.1080/17445647.2017.1290556

Hawkins, S. E., Boldt, J. D., Darlington, E. H., Espiritu, R., Gold, R. E., Gotwols, B., Grey, M. P., Hash, C. D.,

Hayes, J. R., Jaskulek, S. E., & Kardian, C. J. (2007). The Mercury dual imaging system on the MESSENGER spacecraft. *Space Science Reviews*, *131*(1), 247–338. https://doi.org/10.1007/s11214-007-9266-3

Kinczyk, M. J., Prockter, L. M., Byrne, P. K., Susorney, H. C. M., & Chapman, C. R. (2020). A morphological evaluation of crater degradation on Mercury: Revisiting crater classification with MESSENGER data. *Icarus*, *341*, 113637. https://doi.org/10.1016/j.icarus.2020.113637

Kinczyk, M. J., Prockter, L. M., Denevi, B. W., Ostrach, L. R., & Skinner, J. A. (2018). A global geological map of Mercury. In *Mercury: Current and future science of the innermost planet* (Vol. 2047, pp. 6123). LPI Publication. Bibcode: 2018LPICo2047.6123K.

King, J. S., & Scott, D. H. (1990). Geologic map of the Beethoven quadrangle of Mercury. USGS Miscellaneous investigations series Map I–2048.

Mancinelli, P., Minelli, F., Pauselli, C., & Federico, C. (2016). Geology of the Raditladi quadrangle, Mercury (H04). *Journal of Maps*, *12*(sup1), 190–202. https://doi.org/10.1080/17445647.2016.1191384

Marchi, S., Chapman, C. R., Fassett, C. I., Head, J. W., Bottke, W. F., & Strom, R. G. (2013). Global resurfacing of Mercury 4.0-4.1 billion years ago by heavy bombardment and volcanism. *Nature*, *499*(7456), 59–61. https://doi.org/10.1038/nature12280

Marchi, S., Mottola, S., Cremonese, G., Massironi, M., & Martellato, E. (2009). A new chronology for the moon and mercury. *The Astronomical Journal*, *137*(6), 4936–4948. https://doi.org/10.1088/0004-6256/137/6/4936

Pegg, D. L., Rothery, D. A., Balme, M. R., Conway, S. J., Malliband, C. C., & Man, B. (2021). Geology of the Debussy quadrangle (H14), Mercury. *Journal of Maps*, *17*(*2*), 718–729. https://doi.org/10.1080/17445647.2021.1996478

Prockter, L. M., Ernst, C. M., Denevi, B. W., Chapman, C. R., Head, J. W., Fassett, C. I., Merline, W. J., Solomon, S. C., Watters, T. R., Strom, R. G., Cremonese, G., Marchi, S., & Massironi, M. (2010). Evidence for young volcanism on Mercury from the third MESSENGER flyby. *Science*, *329*(5992), 668–671. https://doi.org/10.1126/science.1188186

Prockter, L. M., Kinczyk, M. J., Byrne, P. K., Denevi, B. W., Head IIIJ. W., Fassett, C. I., Whitten, J. L., Thomas, R. J., Buczkowski, D. L., Hynek, B. M., Ostrach, L. R., Blewett, D. T., & Ernst, C. M. (2016). The first global geological map of Mercury. In *47th lunar and planetary science conference* (p. 1245). LPI. Abstract No. 1903. https://doi.org/10.1029/2012JE004154.

Schaber, G. G., & McCauley, J. F. (1980). Geologic map of the Tolstoj quadrangle of Mercury (H-8). USGS Miscellaneous investigations series Map I-1199 1980.

Spudis, P. D., & Guest, J. E. (1988). Stratigraphy and geologic history of Mercury. In F. Vilas, C. R. Chapman, & M. S. Matthews (Eds.), *Mercury* (pp. 118–164). University of Arizona Press.

Tanaka, K. L., Skinner, J. A., & Hare, T. M. (2011). Planetary Geologic Mapping Handbook – 2011. Abstracts of the Annual Meeting of Planetary Geologic Mappers https://ntrs.nasa.gov/archive/nasa/casi.ntrs.nasa.gov/20100017213.pdf

Thomas, R. J., Rothery, D. A., Conway, S. J., & Anand, M. (2014). Mechanisms of explosive volcanism on Mercury: Implications from its global distribution and morphology. *Journal of Geophysical Research: Planets*, *119*(10), 2239–2254.

Trask, N. J., & Dzurisin, D. (1984). Geologic map of the Discovery (H-11) quadrangle of Mercury. USGS Miscellaneous investigations series Map I-1658 1659.

Trask, N. J., & Guest, J. E. (1975). Preliminary geologic terrain map of Mercury. *Journal of Geophysical Research*, *80*(17), 2461–2477. https://doi.org/10.1029/JB080i017p02461

van der Bogert, C. H., Poehler, C., Pozzobon, R., Wright, J., Rothery, D., Hiesinger, H., & Ferrari, S. (2020). Update of the Mapping Standards Document and Geo-stratigraphic Maps Ready for Spectral/Compositional Integration, Planmap, CORDIS EU research results, https://ec.europa.eu/research/participants/documents/downloadPublic?documentIds=080166e5d478cde7&appId=PPGMS

Whitten, J. L., Head, J. W., Denevi, B. W., & Solomon, S. C. (2014). Intercrater plains on Mercury: Insights into unit definition, characterization, and origin from MESSENGER datasets. *Icarus*, *241*, 97–113. https://doi.org/10.1016/j.icarus.2014.06.013

Wright, J., Rothery, D. A., Balme, M. R., & Conway, S. J. (2019). Geology of the Hokusai quadrangle (H05), Mercury. *Journal of Maps*, *15*(2), 509–520. https://doi.org/10.1080/17445647.2019.1625821